A Chemical Solution Deposition Route To Nanopatterned Inorganic Material Surfaces

Monika Kuemmel,[†] Joachim Allouche,[†] Lionel Nicole,[†] Cédric Boissière,[†] Christel Laberty,[†] Heinz Amenitsch,[‡] Clément Sanchez,[†] and David Grosso*,[†]

Laboratoire de Chimie de la Matière Condensée de Paris, Université Pierre et Marie Curie−Paris 6, CNRS, 4 place Jussieu, 75252 Paris cedex 05, France, and Institute of Biophysics and X-ray Structure Research, Austrian Academy of Science, Steyrergasse 17/VI, 8010 Graz, Austria

Received March 6, 2007. Revised Manuscript Received May 3, 2007

TiO_2, Al_2O_3, and ZrO_2 patterns (or masks) composed of ordered nanomotifs of various morphologies (i.e., perforations (craters), rings, canyons, wires, dots, or channels) with typical lateral dimensions of <40 nm and thicknesses below 15 nm are presented. They were simply prepared by chemical solution deposition (CSD) of molecular inorganic precursors and commercial block copolymers on bare or hydrophobised silicon wafer surfaces. The various nanostructures are obtained by self-assembly during evaporation and are subsequently stabilized at 500 °C. Compared to other techniques for surface nanopatterning, the present method has the advantage of being cheap, reproducible, and easy to scale up and does not require specialized equipment. The type, dimension, and organization of these motifs were assessed by AFM, FE-SEM, spectroscopic ellipsometry, and GI-SAXS and are shown to depend on the conditions of preparation. We show that the critical parameters for controlling the nanopattern characteristics are the organic to inorganic ratio, the solvent composition, the substrate surface energy, the evaporation temperature, and the quantity of initial solution deposited on the substrate. XPS investigation was used to access the chemical composition of the nanopatterns on the SiO_2 surface.

1. Introduction

Patterning surfaces leads to the creation of physicochemical heterogeneities (e.g. surface energy, chemical reactivity, conductivity, topography ...), which are an important issue in the design of complex components used in high-tech technologies. Control over the dispersion, organization, and dimension of the domains spread over the surface becomes a special challenge when these fall below 50 nm in size. Methods used to prepare such supported bidimensional networks were mainly developed for the fabrication of optoelectronic and electronic components. For instance, the preparation of ordered single layers of well-dispersed nanoparticles often requires physical techniques that are difficult to perform and that can be applied efficiently only on small surfaces.[1,2] Lithography is certainly the most common and reliable technique to modify surfaces with a high degree of control of the pattern regularity. However, extending such a control below 100 nm is challenging, requiring novel approaches such as dip-pen nanolitography,[3,4] nanosphere lithography,[5] or even ion beam lithography.[6] Another recent approach uses liquid deposition of polystyrene-based block copolymers to create nanoperforated pure polymer layers.[7−9] Other groups have worked on developing the microcontact printing methodologies, but dimensions remain longer than 100 nm.[10]

Here, we expand upon recent progress made in the use of evaporation-induced self-assembly (EISA)[11−13] for nanostructuration of thin films. We successfully form nanopatterns with dimensions of up to 40 nm.[14,15] EISA involves nanotexturation via the liquid deposition of condensable inorganic precursors in the presence of micelle forming surfactants. Such a method is simple, cheap, scaleable, and gives high reproducibility without expensive, specialized equipment. On the other hand, chemical and processing conditions must be

* Corresponding author. Fax: 33 (0) 1 44 27 47 69. Tel: 33 (0) 1 44 27 55 42. E-mail: grosso@ccr.jussieu.fr.
[†] Université Pierre et Marie Curie−Paris 6.
[‡] Austrian Academy of Sciences.

(1) Committee on Challenges for the Chemical Sciences in the 21st Century of the National Research Council, Beyond the Molecular Frontier; *Challenges for Chemistry and Chemical Engineering*, 2004; National Academies Press: Washington, DC, 2004.
(2) Chu, M.-W.; Szafraniak, I.; Scholz, R.; Harnagea, C.; Hesse, D.; Alexe, M.; Gçsele, U. *Nat. Mater.* **2004**, *3*, 87.
(3) Hong, S. Zhu, J.; Mirkin, C. A. *Science* **1999**, *286*, 523.
(4) Zhang, H.; Chung, S.-W.; Mirkin, C. A. *Nano Lett.* **2003**, *3*, 43.
(5) Haes, A. J.; Haynes, C. L.; McFarland, A. D.; Schatz, G. C.; Van Duyne, R. P.; Zou, S. *MRS Bull.* **2005**, *30*, 368.
(6) Zhu, F. Q.; Chern, G. W.; Tchernyshyov, O.; Zhu, X. C.; Zhu, J. G.; Chien, C. L. *Phys. Rev. Lett.* **2006**, *96* (2), 027205/1.
(7) Spatz, J. P.; Roescher, A.; Moller, M. *Adv. Mater.* **1996**, *8*, 337.
(8) Glass, R.; Moller, M.; Spatz, J. *Nanotechnology* **2003**, *14*, 1153−1160.
(9) Sun, Z.; Wolkenhauer, M.; Bumbu, G.-G.; Kim, D. H.; Gutmann, J. S. *Physica B* **2005**, *357*, 141.
(10) Husemann, M.; Mecerreyes, D.; Hawker, C.; Hedrick, J.; Shah, R.; Abbott, N. *Angew. Chem., Int. Ed.* **1999**, *38*, No. 5, 647.
(11) Brinker, C. J.; Lu, Y.; Sellinger, A.; Fan, H. *Adv. Mater.* **1999**, *11*, 579.
(12) Grosso, D.; Cagnol, F.; Soler-Illia, G. J. A. A.; Crepaldi, E.; Amenitsch, H.; Brunet-Bruneau, A.; Bourgeois, A.; Sanchez, C. *Adv. Funct. Mater.* **2004**, *14*, 309.
(13) Grosso, D.; Boissiere, C.; Nicole, L.; Sanchez, C. *J. Sol−Gel Sci. Technol.* **2006**, *40* (2/3), 141.
(14) Grosso, D.; Boissière, C.; Smarsly, B.; Brezinsky, T.; Pinna, N.; Albouy, P. A.; Amenitsch, H.; Antonietti, M.; Sanchez, C. *Nat. Mater.* **2004**, *3*, 787.
(15) Fisher, A.; Kuemmel, M.; Järn, M.; Linden, M.; Boissière, C.; Nicole, L.; Sanchez, C.; Grosso, D. *Small* **2006**, *2*, No.4, 569.

10.1021/cm0706245 CCC: $37.00
Published on Web 06/23/2007

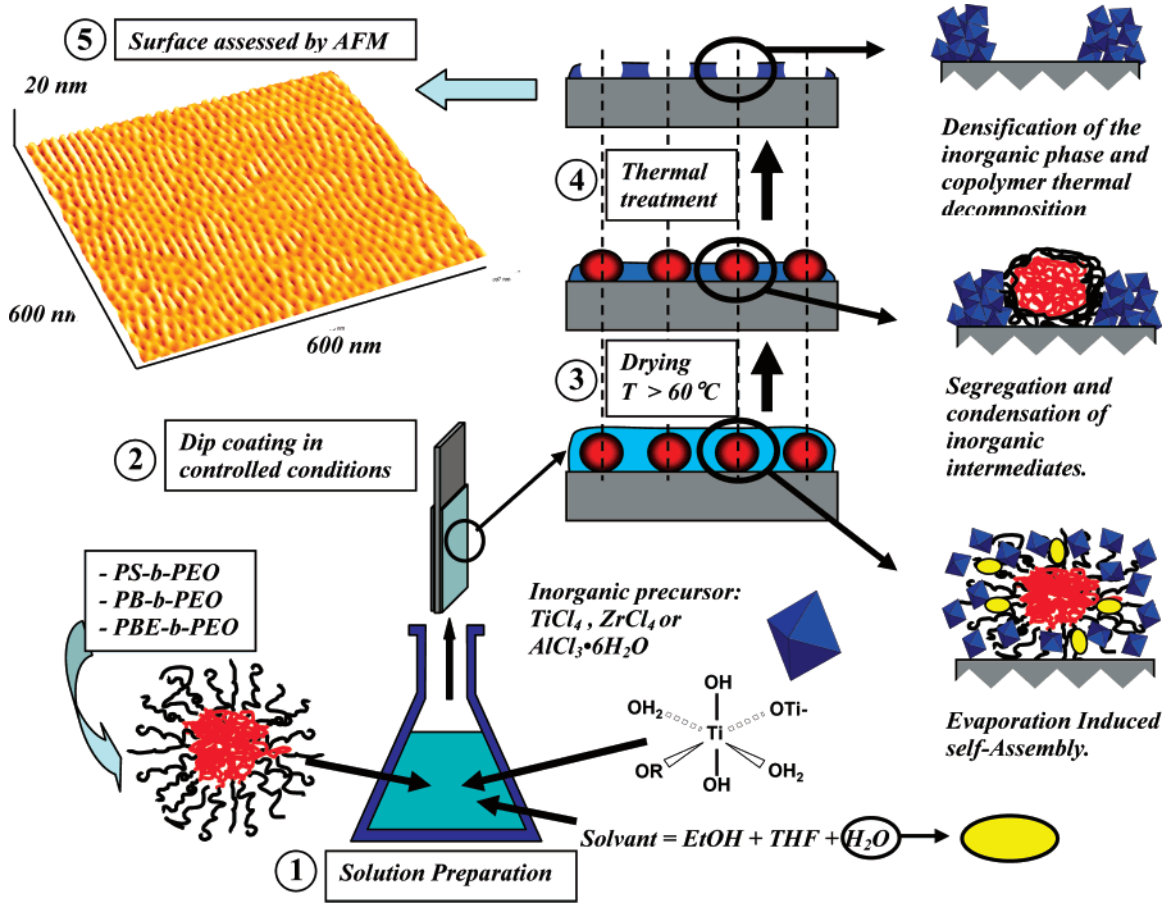

Figure 1. Scheme describing the principle of the metal oxide nanopattern (mask) preparation from inorganic precursors and block copolymers. The above AFM image corresponds to sample TiBE-P23 (see Table 1).

well-controlled in order to optimally achieve highly ordered patterns. It is also important to use specific amphiphilic block copolymers that are large enough (MW > 20 000 g mol^{-1}) and contain at least two blocks with strong hydrophilicity contrast, with polyethyleneoxide usually chosen as hydrophilic chains as a result of its high compatibility with hydrosoluble cations.[13,16] In a recent work, we reported the formation of TiO_2 ultrathin layers bearing nanoperforations through which the SiO_2 substrate surface was accessible.[15] These perforations (or craters) were homogeneously distributed within the titania layer, forming well-ordered nanopatterns. Their dimension was adjusted between 10 and 30 nm in diameter by varying the copolymer molecular weight. A local selective functionalization was investigated to confirm the double nature of the surface. Cheng and Guttmann used the same templating approach to synthesize films with different nanostructures from different structuring agents and TiO_2 precursors.[17] However, the reported structures were not very well ordered and no proof of physical thickness was reported.

In the present article, we describe the preparation of TiO_2, Al_2O_3, and ZrO_2 nanostructured patterns, which can be considered nanomasks, composed of various type of nanomotifs (i.e., perforations (also addressed as craters), rings, canyons, wires, dots, or channels) that are homogeneously dispersed on the substrate. Correlation distances between periodic motifs were less than 50 nm. Figure 1 illustrates the method used to prepare such systems. The advantages of such oxide patterns over the pure polymer ones are improved mechanical resistance, chemical inertness, and thermal stability. We show that solvent polarity, organic to inorganic ratio, dilution, temperature, dissolution conditions, and substrate surface energy are critical parameters for controlling the nanostructure of these patterns. The influence of each of these parameters on the formation of the patterns is discussed. These ceramic-based nanopatterns are novel highly ordered heterogeneous substrates that contain well-dispersed nanosites for heterogeneous nucleation. These sites, or nanobeakers, are not only defined by their chemical heterogeneity, but are mechanically confined by the presence of the surrounding ceramic nanowalls.

2. Experimental Section

2.1. Initial Solutions. Absolute ethanol and THF were purchased from Normapur. Inorganic precursors (e.g., $TiCl_4$, $ZrCl_4$, and $AlCl_3 \cdot 6H_2O$) were purchased from Aldrich and used without further purification. The PS-*b*-PEO (polystyrene-*b*-polyethyleneoxide, P4750-SEO; $MW_{PS} = 40\,000$ g mol^{-1}, $MW_{PEO} = 36\,000$ g mol^{-1}), and PB-*b*-PEO (polybutadiene-*b*-polyethyleneoxide, P2325-BdEO; $MW_{PB} = 32\,000$ g mol^{-1}, $MW_{PEO} = 43\,500$ g mol^{-1}) polymers were purchased from Polymersource and used as received. The PBE-*b*-PEO (hydrogenated polybutadienecoethylene-*b*-polyethyleneoxide,

(16) de A. A. Soler-Illia, G. J.; Crepaldi, E. L.; Grosso, D.; Sanchez, C. *Curr. Opin. Colloids Interface Sci.* **2003**, *8*, 109.
(17) Cheng, Y.-J.; Gutmann, J. S. *J. Am. Chem. Soc.* **2006**, *128* (14), 4658.

Table 1. Chemical and Processing Conditions for Elaboration of Patterns and Their Characteristics[a]

	initial solution composition				dipping conditions		system characteristics		
sample	R_{polym}	R_{THF}	R_{EtOH}	R_{H_2O}	T (°C)	S (mm s^{-1})	H (nm)	D (nm)	P (nm)
TiS-P12	4.4	176	176	3.5	25	1.2	5 ± 2	12	
TiS-C10	4.4	176	70	3.5	25	1.2		10	
TiS-R10	4.4	176	220	3.5	25	1.2		10[e]	
TiB-P33	0.22		88	11[b]	60	0.44	10 ± 1	33	45
TiB-P14	0.22	40	66	2.2	60	0.44		14	30
TiBE-P12	0.39	34	92	2.6	60	0.44	7 ± 2	12 (23[c])	28
TiBE-P15	1.47	24	62	1.1	25	1.7	8 ± 2	15	27
TiBE-D23[d]	1.47	24	62	1.1	25	1.7		23	30
TiBE-W13	2.55	13	86	1	25	1.4		13	
TiBE-CH15	0.40		79	6.3	25	0.8		15	
AlS-P12	0.16	22	18	1.34[f]	25[g]	0.7	4 ± 2	12	24
ZrB-P10	0.14	26	43	2	60	0.44	6 ± 2	10	17

[a] Samples are labeled starting with the cation (Ti, Al, or Zr), followed by the hydrophobic polymer chain (S, B, and BE for polystyrene, polybutadiene, and polybutadienecoethylene, respectively). The second part of the label addresses the type of motif (P = perforation, C = canyon, R = rings, D = dot, W = wire, CH = channel) and the size of the motif in nanometers. R values correspond to weight ratios with respect to the precursor weight (e.g., $R_{H_2O} = m_{H2O}/m_{(MCln,\ mH2O)}$); T and S correspond to the temperature during evaporation and to the dipping speed, respectively. The pattern characteristic dimensions were deduced from AFM images (care must be taken with these analyses, because they have been done in noncontact mode) and ellipsometry. They are given by H for the average thickness, D for the motif lateral dimension, and P for the motif periodicity. [b] Aqueous solution of HCl (10% weight). [c] Determined from FE-SEM image. [d] Hydrophobic substrate. [e] Internal diameter. [f] Aqueous solution of NH_3 (15% weight). [g] Evaporation took place at 22% relative humidity.

KLE-29;[18] $MW_{PBE} = 12\,000$ g mol^{-1}, $MW_{PEO} = 25\,000$ g mol^{-1}) was provided by the Max Planck Institute of Colloids and Interface Sciences of Golm (Germany). Si wafers were cut into 1 cm × 3 cm pieces and treated in a 3 M HNO_3 aqueous solution for 1 day before being rinsed with water and ethanol and stored in deionized water. Just before deposition, substrates were removed from water, rinsed with EtOH, and wiped dry with a tissue soaked with acetone. Hydrophobic substrates, used to obtain the TiBE-D23 type of patterns (see Table 1), were prepared by grafting dodecyl groups on the substrate surface. To do so, clean pieces of silicon wafers were left for 120 min in EtOH/1% dodecyltriethoxysilane, before being rinsed with ethanol and dried at 130 °C for 24 h. Preparation of initial solutions involves the addition of a first solution A, composed of the copolymer dissolved in part of the solvent, to a second solution B, composed of the inorganic precursor dissolved in the remaining part of the solvent. Water must be added in solution A if no THF is present in the final composition in order to facilitate the dissolution of the copolymer. For the Al-based system, water/NH_3 must be added in solution B, which additionally requires at least 2 weeks of aging, to favor the precondensation of the $Al(H_2O)_6$ species. In all cases, after mixing of A and B, stirring of at least 30 min was allowed before deposition. Final solution compositions are presented in Table 1.

2.2. Film Preparation. Films were deposited at a constant withdrawal rate (see Table 1), in relative humidity <10% (except for Al_2O_3), and at constant temperature of 25 or 60 °C. Films were directly transferred underneath a curing IR lamp (500 °C at the sample surface) so as to complete the inorganic condensation of the matrix and to decompose the block copolymer template.

2.3. Characterization. Pattern topography and nanostructure were deduced from atomic force microscopy (AFM) investigations performed with a Veeco DI-CPII in noncontact mode. Field-emission scanning electron microscopy (FE-SEM Hitachi S4200) was used to confirm the AFM results. Long-range periodicity and thickness homogeneity were assessed by grazing incident small-angle X-ray scattering (GI-SAXS) conducted at the Austrian SAXS beam line of Elettra synchrotron (Italy). Samples were placed under the beam at an incident angle of 0.2°. Scattering patterns were collected on an X-ray-sensitive CCD camera (energy, 8 keV; beam size, 400 μm; sample−detector distance, 130 cm; acquisition time, 2 min). The thickness of films was measured in dry air at ambient temperature by variable-angle spectroscopic ellipsometry (VASE Woolam 2000U) at an incidence angle of 70° in the spectral range of 400−1000 nm. The Bruggeman effective medium approximation was used to estimate the volume fraction of air associated with the motifs. Surface chemical compositions were analyzed by X-ray photoelectron spectroscopy (XPS−ESCALAB 250, Al Kα (1486.6 eV) source; take off angle = 90°). The presence of micelles in the precursor solutions were evaluated by quasielastic light-scattering (QELS) analysis using a Brookhaven apparatus ($\lambda = 632$ nm; detection angle = 90°).

3. Results and Discussion

3.1. Formation Mechanism. The principle of pattern formation is illustrated in Figure 1. The nanostructure periodicity is associated to the self-assembly of copolymer micelles on the surface, whereas their thermal decomposition is eventually responsible for the creation of the void motifs such as the nanoperforations. Such a mechanism was already proposed in our first report and is now experimentally confirmed by the AFM images in Figure 2 that correspond to the TiS-P12 pattern. After 10 min at 200 °C, well-dispersed polymer particles are clearly observed on the surface, confirming that the PS core has not yet been decomposed. On the other hand, after 10 min at 500 °C, the perforations are visible at the former location of the polymer dots with corresponding dimension and dispersion. In the first step, the temperature rises up to 200 °C, inducing inorganic condensation, whereas the PEO polymer chains become less hydrophilic because of a conformation change

(18) Thomas, A.; Schlaad, H.; Smarsly, B.; Antonietti, M. *Langmuir* **2003**, *19*, 4455.

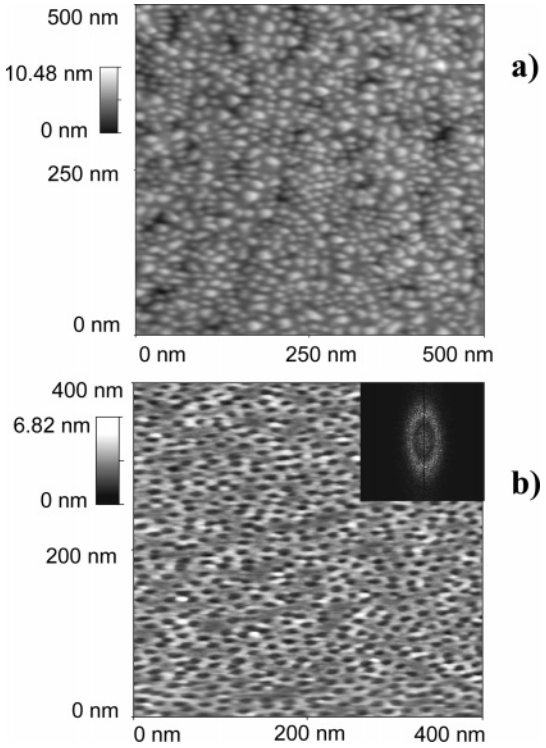

Figure 2. AFM images showing a TiS-P12 (TiO_2) nanomask (motif = perforation) after treatment at (a) 200 °C for 10 min and (b) 500 °C for 10 min. The white dots observed at 200 °C correspond to the PS core of the micelles, whereas at 500 °C, they are fully decomposed, freeing the perforations (see Table 1 for detailed conditions).

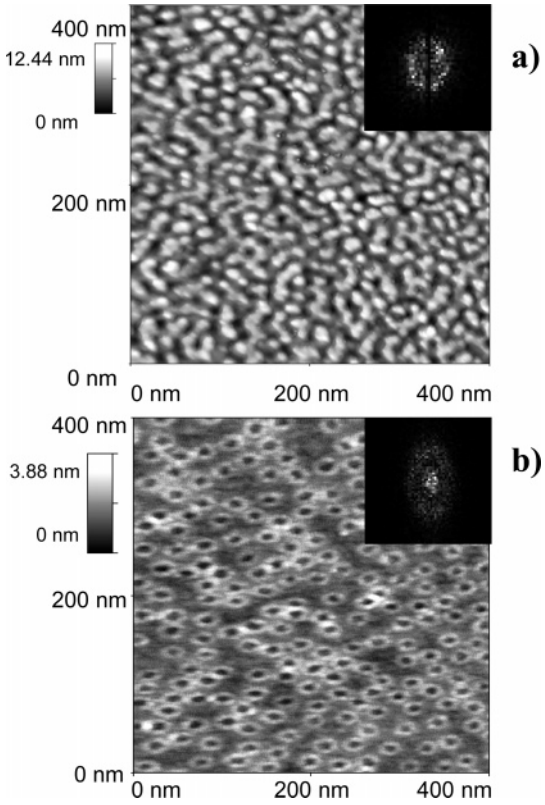

Figure 3. AFM images showing TiO_2 patterns after 10 min at 500°: (a) TiS-C10, disordered nanocanyon patterns obtained under low EtOH conditions; and (b) TiS-R10, well-dispersed nanorings obtained with high EtOH conditions. Intermediate composition leads to nanoperforations shown in Figure 2b (see Table 1 for full conditions).

of the EO units.[16,19,20] Both effects promote the depletion of hydrosoluble species (water and inorganic precursors) from the micelle shell region. The inorganic phase condenses between the polymer micelles on the surface of the substrate. Polymer micelles thus become protuberances that are clearly visible in Figure 2a. Increasing the temperature up to 500 °C causes the complete degradation of the copolymer; leading to the formation of nanocavities at the locations formerly occupied by polymer micelles (see Figure 2b).

3.2. Thickness Evaluation. Thicknesses were difficult to assess by AFM, because analyses were performed in non-contact mode. Ellipsometry analyses give thickness values that are reported in Table 1. These values were between 4 and 10 nm, which is in agreement with what one would expect for deposition of a monolayer of copolymer micelles. An accurate value of the thickness cannot be determined by this latter technique because it is model-dependent and the layer is not plain but has to be seen as an approximation of an effective medium composed of oxide and air. One of the main challenges associated with the formation of these patterns is the verification that a single layer has effectively been deposited. Such a point will be addressed later in the article, when GISAXS data is presented.

3.3. Pattern Morphologies and Dimensions. The nanopattern morphologies are illustrated by AFM images of Figures 3−5 and typical corresponding dimensions are reported in Table 1. These were all obtained on samples that were thermally treated in air at 500 °C for 10 min. Each one of the images is representative of the whole sample surface. We will show that by varying the utilized copolymer as well as the chemical and processing conditions applied, various degrees of organization and morphologies can be formed at the substrate interface (See Table 1).

In all cases, the copolymer is responsible for the observed texturation, because dimensions of the periodic motifs (10−40 nm as observed by AFM) correspond to the dimensions of the copolymer micelles. Micelle dimensions were measured by quasielastic light-scattering (QELS) analysis of the precursor solutions, giving values between 20 and 80 nm. Such dimensions are consistent with estimates on the basis of on their molecular weight and previous works.[19,15,21]

Influence of the Medium (Polarity and Dilution). It has been demonstrated that the formation of mesoporous ordered thin films by evaporation-induced self-assembly (EISA)[11] can be achieved regardless of whether the block copolymer is already micellized or fully solvated in the initial solution. Micellization is dependent on the relative solubility of both chains in the solvent as well as on their relative length. Phase diagrams of PS-*b*-PEO and PB-*b*-PEO block copolymers dispersed into media composed of one or two different solvents have been described by polymer chemists.[22−25] They

(19) Jonsson, B.; Lindman, B.; Holmberg, K.; Kronberg, B. *Surfactants and Polymers in Aqueous Solution*; John Wiley & Sons: Chichester, UK, 1998.
(20) Kipkemboi, P.; Fogden, A.; Alfredsson, V.; Flodstrom, K. *Langmuir* **2001**, *17*, 5398.
(21) Smarsly; Grosso, D.; Brezesinski, T.; Boissière, C.; Pinna, N.; Sanchez, C.; Antonietti, M. *Chem. Mater.* **2004**, *16*, 2948.
(22) Cameron, N.; Corbierre, M.; Eisenberg, A. *Can. J. Chem.* **1999**, *77*, 1311.

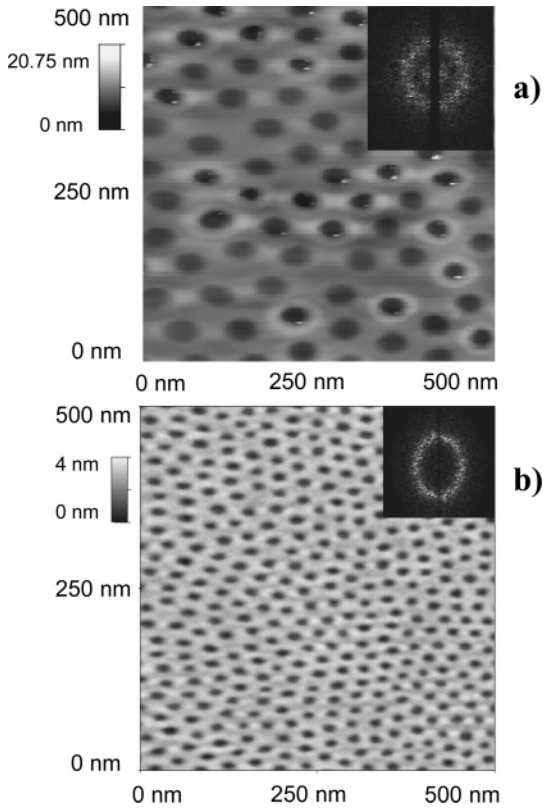

Figure 4. AFM images showing TiO_2 patterns (masks) after 10 min at 500°: (a) TiB-P33, dispersed nanoperforations with large diameter (33 nm) obtained without THF; and (b) TiB-P14, well-ordered nanoperforations with small diameter (15 nm) obtained with THF (see Table 1 for full conditions).

show that the micelle dimension and morphology can be tuned by adjusting the solubility of the macromolecular chains through careful selection of the solvent composition. A similar behavior is observed in the present case, in which the medium additionally contains ionic species and inorganic precursors. Indeed, the following study has been conducted on TiO_2 patterns prepared with PS-*b*-PEO as a template in a mixture of THF, EtOH, and H_2O. PS is highly soluble in THF, poorly soluble in EtOH and not soluble in H_2O as a result of the difference of polarity of these solvents. On the other hand, PEO is highly soluble in THF, EtOH, and H_2O. We started our observation with a THF solution containing fully dissolved PS-b-PEO copolymer (in the proportion of Table 1, the influence of the small fraction of water can be neglected). This solution turns turbid when the inorganic precursor solution in EtOH is progressively added as a result of the micellization of the copolymer. Too much EtOH induces its precipitation. Using a good solvent for both polymer chains and then adding a poor solvent for one of them is a known way for the preparation of "crew-cut" aggregates of block copolymers.[22] It can thus successfully be used to vary the micelle morphology in an inorganic chemical solution. To illustrate the richness of this approach, we analyzed patterns prepared with different EtOH contents by AFM.

In the conditions of the TiS-XXX systems, formation of homogeneous patterns starts at R_{EtOH} above 60 (See Table 1). When $60 < R_{EtOH} < 140$, interconnected canyon motifs as in Figure 3a are observed. When $140 < R_{EtOH} < 200$, well-dispersed and discrete perforations of homogeneous dimension are formed (see Figure 2a). When $200 < R_{EtOH} < 240$, patterns are composed of well-separated nanorings, as clearly observed in Figure 3b. Above $R_{EtOH} = 240$, the copolymer is nonsoluble and no films could be prepared. Two distinct influences can be pointed out. First, well-dispersed and separated motifs are formed only when micelles are formed in the solution, prior to deposition. When no micelles are formed, micellization or segregation occurs on the surface, as for thicker films in previous reports.[21] In the present conditions of fast evaporation (low quantity of solution and low humidity), such large copolymer chains have difficulties completing the self-assembly, which leads to the observed poorly defined structures. Second, high values of R_{ETOH} produce a noncontinuous, but homogeneous, layer of dispersed rings that is associated with the higher dilution. The ring morphology indicates that the inorganic precursors were situated in the hydrophilic PEO shells of the micelles at the moment of deposition.

Medium polarity affects not only the formation of micelles but also the size of the formed micelles. Indeed, we will show that after changing the block copolymer to PB-*b*-PEO, which can be stabilized in the form of micelles in EtOH/water mixtures in the conditions of Table 1, we can change the size of the perforations by changing the polarity of the solvent. This is illustrated by Figure 4, where the copolymer solubility was increased by replacing a fraction of EtOH with THF and reducing the proportion of water. This difference results in the formation of smaller perforations, 14 nm in diameter instead of 33 nm. This can be explained by the fact that solvation systems with a higher dissolution capacity can accommodate smaller micelles with higher curvatures (larger surface-energy contribution). This is confirmed by QELS analysis, which shows that micelles in solution grow significantly upon the addition of inorganic precursors and EtOH (e.g., from 28 to 48 nm in the case of TiB-P14). The cations may also influence the conformation of the PEO chains.

Influence of Inorganic/Organic Proportion. Previous work on mesoporous thin films highlighted the importance of the inorganic/organic ratio on the final mesostructure.[12,26] The AFM image in Figure 5a shows that when using a relatively similar volume fraction of both phases (TiO_2 and copolymer densities are considered), classical perforations are formed. Increasing the proportion of copolymer in the solution (See Figure 5c) leads to the formation of larger polymer domains and, after thermal treatment, to uncovered areas that are not homogeneous in shape. On the other hand, the nanowalls (interconnected wires) of TiO_2 separating these domains do have a homogeneous dimension that is close to that measured for nanoperforated patterns. The reason for this behavior is not fully understood yet. According to these results, we suggest that when a too low ratio of TiO_2 to

(23) Svensson, M.; Alexandridis, P.; Linse, P. *Macromolecules* **1999**, *32*, 637.
(24) Bronstein, L.; Chernyshov, D.; Timofeeva, G.; Dubrovina, L.; Valetsky, P. *Langmuir* **1999**, *15*, 6195.
(25) Förster, S.; Berton, B.; Hentze, H.-P.; Krämer, E.; Antonietti, M. *Macromolecules* **2001**, *34*, 4610.
(26) Crepaldi, E. L.; de A. A. Soler-Illia, G. J.; Grosso, D.; Cagnol, F.; Ribot, F.; Sanchez, C. *J. Am. Chem. Soc.* **2003**, *125*, 9770.

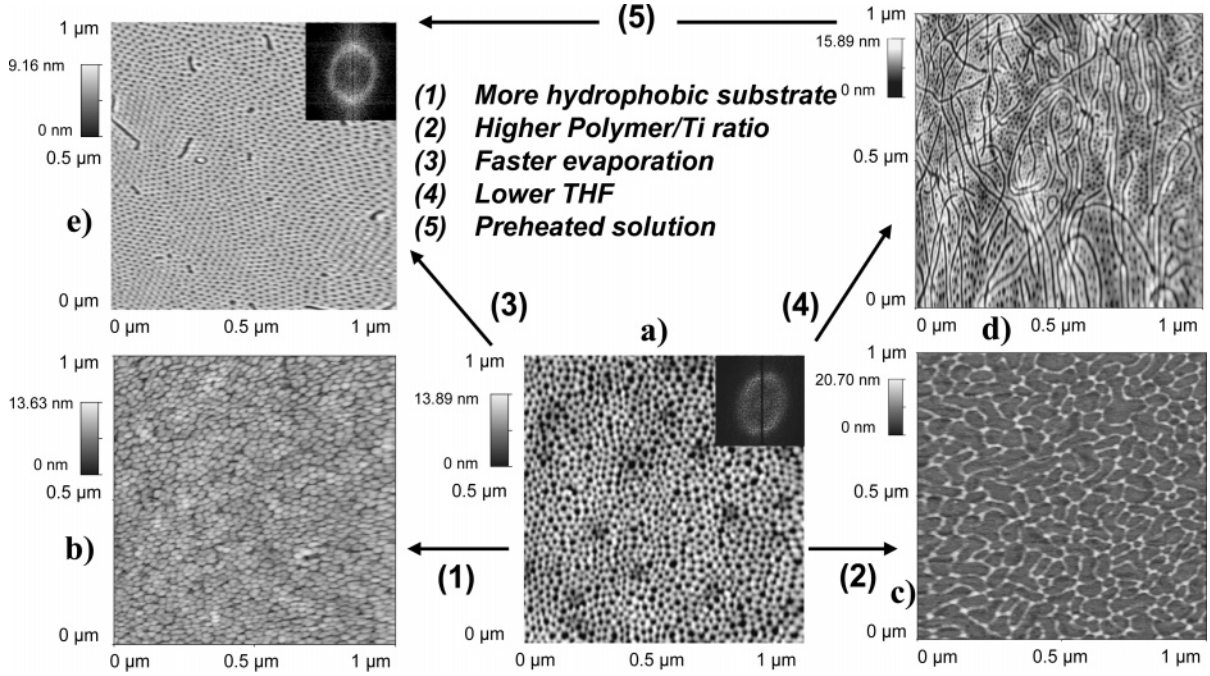

Figure 5. AFM images showing PBE-*b*-PEO-templated TiO_2 nanomasks and nanopatterns after 10 min at 500°: (a) TiBE-P15, dispersed nanoperforations; (b) TiBE-D23, dispersed nanodots; (c) TiBE-W13, dispersed connected nanowires; (d) TiBE-CH15, coexistence of nanoperforations and nanochannels; and (e) TiBE-P12, highly ordered nanoperforations. The differences between samples are expressed by transition arrows from (1) to (5). The changes concern (1) the substrate surface, (2) the organic/inorganic ratio, (3) the evaporation temperature, (4) the solvent, and (5) solution conditioning (see Table 1 for detailed conditions).

copolymer species is used, deposited micelles cannot be stabilized as such on the surface. The system will thus reduce the contribution of the surface energy by decreasing the inorganic/organic interface area through coalescence of micelles into larger copolymer domains. One may see this transformation as a spinodal phase separation taking place on a surface. This phenomenon gives rise to organic domains, void after decomposition, surrounded by TiO_2 walls or wires.

Influence of Substrate Surface. Because all micelles are interacting directly with the surface of the substrate, the nature of the latter must strongly affect the morphology of the pattern. All substrates were silicon wafers bearing a native layer of SiO_2 on their surface. The pretreatment (see Experimental Section) aims at increasing the surface energy so as to favor interaction of hydrophilic titania and the PEO shell of the micelles with the surface. When modifying the surface by grafting a hydrophobic dodecyl group (before deposition of the patterns, substrates nongrafted and grafted with dodecyl groups, as described in the Experimental Section, show water contact angles of 23 and 95°, respectively), dispersed dots with a dimension characteristic of the copolymer micelles are formed (see Figure 5b). In these conditions, titania precursors and PEO chains do not interact favorably with the surface. Only the hydrophobic part of the micelles is likely to interact with the alkyl chains of the surface, resulting in either hemispherical or inverse micelles deposited on the hydrophobic substrate.[27] The TiO_2 precursors gather within the PEO-rich regions of the micelles. After thermal treatment, monolayers of well-dispersed TiO_2 dots are formed, confirming the critical influence of the substrate surface energy.

(27) Aksay, I.; Traun, M.; Manne, S.; Honma, I.; Yao, N.; Zhou, L.; Fenter, P.; Eisenberger, P.; Gruner, S. *Science* **1996**, *273*, 892.

Influence of Temperature. The temperature of evaporation seems to have no effect on the micelle morphology but has a critical role on their organization within the pattern. Comparing AFM images a and e of Figure 5 reveals the influence of increasing the evaporation rate by applying a temperature of 60°. The degree of ordering of the nanoperforations is greater than at room temperature, whereas the periodicity is not significantly modified. A higher temperature tends to decrease the viscosity of the solution layer just after deposition, which results in an increase of the species mobility in the solution. The combination of faster evaporation and greater mobility is likely to be responsible for the increased degree of ordering. Higher temperature is also associated with higher solubility. As already observed, higher solubility leads to smaller perforations, which is confirmed in the present case ($D = 12$ nm at 60 °C against $D = 15$ nm at 25 °C). The FE-SEM photo in Figure 6 confirms the typical periodicity of TiBE-P12. The average perforation size is greater than when measured by AFM as a result of the resolution limitation of both techniques.

Influence of Solution Conditioning. Nanochannels (TiBE-CH15, Figure 5d) were obtained when elongated micelles were supposedly present in the solution previous to deposition. QELS shows two populations centered at several hundred and several thousand nanometers, respectively, corresponding to elongated micelles, in addition to a population around 50 nm, which corresponds to the spherical micelles also found in the other samples. Such mixed systems have also been evidenced by Eisenberg and co-workers for a system of PS-*b*-PMAA.[22] In mesophases, elongated cylindrical micelles have lower interface curvatures with their environment than spherical micelles, which reflects a lower solubility of the core parts. This is generally obtained by

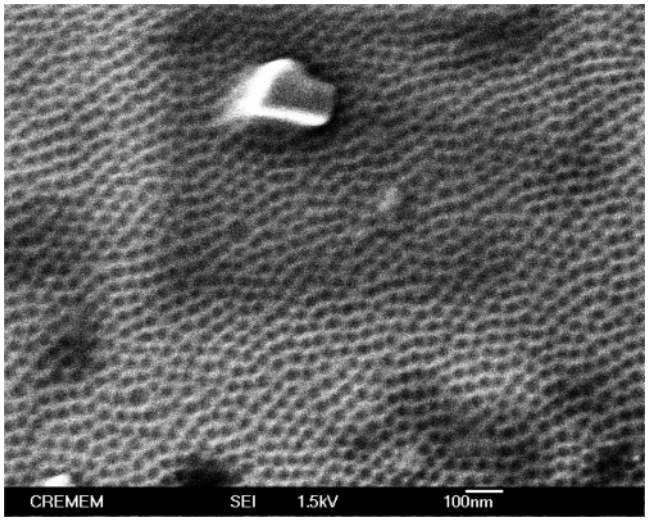

Figure 6. FE-SEM image showing well-ordered nanoperforations of pattern TiBE-P12 (see Table 1 for full conditions).

increasing the concentration or by decreasing the dissolution capacity of the medium. Here, channels are found in the patterns when the initial solution is rich in water and poor in THF, reducing the solubility of the copolymer. These elongated micelles disappear from the patterns, and presumably from the solution, when the solution is heated to 80 °C for at least 30 min and cooled before deposition. Such a procedure allows for a re-homogenization of the micelles (see transition 5 in Figure 5). This observation underlines the importance of the solution pretreatment before coating. Indeed, such large macromolecules of copolymer have reduced entropy, and thermodynamic equilibrium and stable copolymer aggregation states are sometimes difficult to attain. Micelle size and morphology in the solution may thus change with time. The presence of both spherical and elongated micelles in TiBE-CH15 patterns is evidence of such an evolution of the solution (coexistence of domains is possible only for a first-order transition mechanism, which is the case for the mesophase systems).

Influence of Solution Aging Time. Solutions contain inorganic TiO_2 precursors consisting of titanium-oxo-oligomers stabilized by the high acidity of the media. In a previous article, we demonstrate that $TiCl_4$ reactants are partially hydrolyzed and do not contain any chloride in their coordination sphere under the present conditions.[26] The stability of these intermediates is relative. Formation of larger oxo clusters and finally colloidal nanoparticles of TiO_2 with lower mobility occurs with time. As a result, the quality of crater formation is reduced with aging time. Better organized craters that are more monodisperse in size are obtained with young solutions (within 1 week), whereas a 1 month old solution produces craters of lower quality. In view of the influence of the solution conditioning, more reproducible results were obtained by stocking the solutions at −20 °C. Solutions can then be heated for 30 min at 80 °C to achieve homogenization. In addition, fresh solutions are preferred to used solutions because part of the solvent evaporates during pattern processing.

Influence of Humidity. Humidity during dip-coating is a critical variable that may assist or perturb the self-assembly

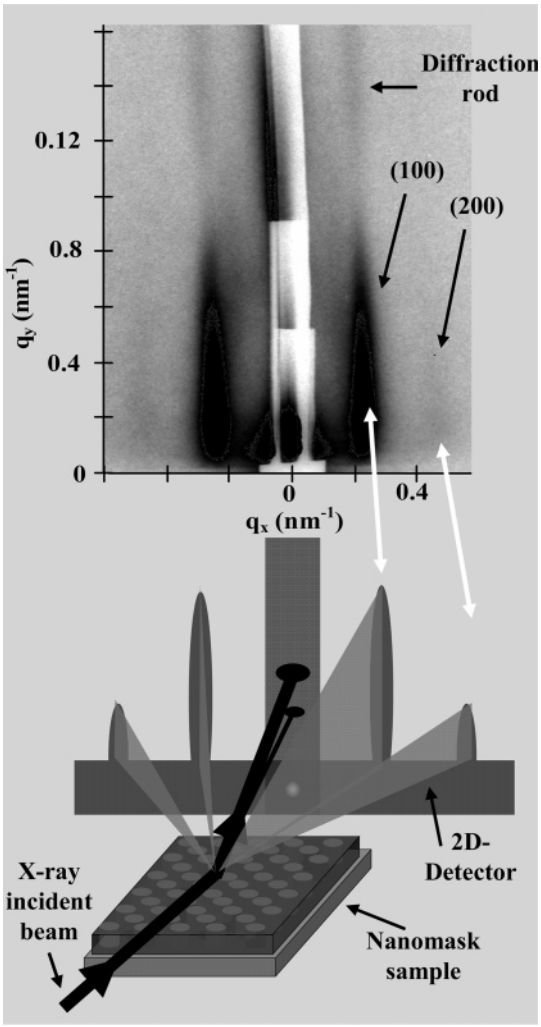

Figure 7. GI-SAXS investigation of TiO_2 TiBE-P12 pattern after 10 min at 500 °C.

by modifying the evaporation speed and the equilibration of the film's water content with its environment.[28] For TiO_2 patterns, a low relative humidity (often associated with a high temperature) is preferred in order to favor a fast evaporation often needed for the formation of homogeneous dispersions. Varying the relative humidity up to 80% after complete evaporation did not lead to a modification of the nanostructure.

3.4. GISAXS Investigation. The GI-SAXS diagram of the highly ordered nanoperforated pattern observed for the TiBE-P12 sample (Figure 5e) is displayed in Figure 7. Much morphological information can be extracted from the scattered radiations. First, intense in-plane Bragg diffractions and their corresponding second order are collected at $q_{x1} = 0.22$ nm^{-1} and $q_{x2} = 0.44$ nm^{-1}, respectively. These diffractions correspond to highly ordered motifs distributed on the surface of the substrate with a characteristic separating distance of 28 nm, which is in agreement with previous topological studies. The presence of the second order is associated with a high degree of ordering. The X-ray incident beam was 400 μm wide, which suggests that a wide surface of the sample

(28) Cagnol, F.; Grosso, D.; de A. A. Soler-Illia, G. J.; Crepaldi, E. L.; Babonneau, F.; Amenitsch, H.; Sanchez, C. *J. Mater. Chem.* **2003**, *13*, 61.

was irradiated. Because only one narrow diffraction signal was recorded in the x direction, one supposes that the perforations motifs are homogeneously distributed on the whole surface.

The second information of great importance is extracted from the extensions of the off-plane diffracted signal in the *y* direction. These are called diffraction rods and are characteristic of a monolayer of motifs spread over a surface. At increasing values of q_y, the diffraction rods decrease in intensity before regaining intensity. This is related to interference construction and destruction associated with the propagation of the diffracted signal in the layer (Kiessig fringes from diffracted radiations). The second rods observed at higher q_y values are thus the harmonics of rods collected at low q_y values. Their presence confirms the high homogeneity of the monolayer thickness. Modelization of the diffracted rod signal profile revealed that layer thicknesses are around 10 nm, which is close to the value of 7 ± 2 nm determined by ellipsometry. A precise determination of the motif morphology and of the thickness is possible through the determination of the form factor associated with the scattered signals. Such an investigation could not be performed with the diagram of Figure 7, but will be done with future GI-SAXS patterns that will be recorded with higher resolution during an upcoming synchrotron beam time.

3.5. Extension to Other Oxide Patterns. It has been shown previously that EISA methods can be used to produce thick and thin mesoporous metal oxide films, among which Al_2O_3[29] and ZrO_2[30] are of prime importance because of their optical transparency and their electrical resistivity. Figure 8 displays the AFM images of aluminum oxide and zirconium oxide-based patterns (masks) with well-dispersed homogeneous perforations. Similar topological characteristics to TiO_2-based patterns are evident. This confirms that the presented method for nanopattern structuration can be extended to other inorganic systems.

3.6. Chemical Composition of the Surface. To assess the chemical composition, we have analyzed the surfaces of the TiBE-P12 and AlS-P12 systems by XPS. Results confirm the presence of TiO_2 and Al_2O_3 patterning on the SiO_2 surface, because chemical shifts correspond to the expected chemical environment for both phases. For the TiBE-P12 sample, peaks with binding energy corresponding to O1s (530 eV) from Ti−O, Si2p (102.3 eV) from SiO_2, and Ti2p (458.7 and 464.4 eV) from TiO_2 were observed. An additional O1s peak is observed as a shoulder at a binding energy of 531.7 eV, which can be attributed to OH groups or oxygen from SiO_2. This latter signal disappears after 3 min of argon etching at an intensity of 5 μA, which suggests that this treatment is sufficient to remove both OH groups and the SiO_2 sublayer (bottom of the perforation) from the sample surface. The AlS-P12 spectrum exhibits peaks with binding energies corresponding to O1s (531.9 eV) from Al−O, Si−O, and OH groups, Si2p (102.3 and 98.8 eV) from SiO_2 and pure Si (substrate), and Al2p (74.4 eV), which is consistent with a hydrated aluminum transition oxide phase ($AlO_{(1.5-x)}(OH)_{2x}$). Si/(Si+Al) atomic fractions were 65 and 75% before and after etching, respectively, whereas the Si/(Si+Ti) atomic fraction increases from 36 to 50% upon etching. These atomic fractions confirm the accessibility of the substrate surface through the perforations. On the other hand, they may not correspond exactly to the real fraction of accessible substrate surface (bottom of the perforations), because the X-ray probing depth is not exactly known. Chemical analyses were investigated by wide-angle XRD, RAMAN spectroscopy, and FTIR, but no additional information could be deduced as a result of the extremely low quantity of material.

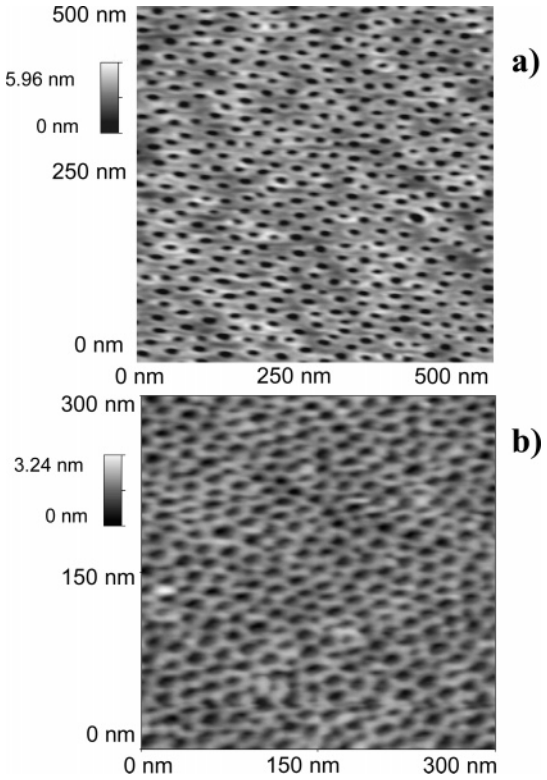

Figure 8. AFM images showing masks (motifs = nanoperforations) after 10 min at 500°: (a) Al_2O_3 layer templated with PS-*b*-PEO (AlS-P12) and (b) ZrO_2 layer templated with PB-*b*-PEO (ZrB-P10) (see Table 1 for full conditions).

4. Conclusions

We present a general method for preparing highly ordered nanopatterns of various oxides by simple chemical solution deposition using commercial copolymers. We demonstrate that several types of motifs (i.e., perforations (craters), rings, canyons, wires, dots, or channels) can be homogeneously distributed within the ceramic monolayer by controlling the condition parameters. Among these, the evaporation conditions and the aggregation state of the copolymer in the solution, mainly governed by the polarity of the solvent and the solution conditioning, are shown to be crucial. Additional work is conducted to better understand the behavior of these copolymers in such complex solutions. These heterogeneous nanostructured surfaces, such as dispersed nanobeakers, are currently being tested in our laboratory as novel substrates for various applications.

(29) Kuemmel, M.; Grosso, D.; Boissière, C.; Smarsly, B.; Brezinski, T.; Albouy, P. A.; Amenitsch, H.; Sanchez, C. *Angew. Chem.* **2005**, *44*, 4589.
(30) Crepaldi, E. L.; de A. A. Soler-Illia, G. J.; Bouchara, A.; Grosso, D.; Durand, D.; Sanchez, C. *Angew. Chem.* **2002**, *3*, 347.

Acknowledgment. We thank the European Network of Excellence FAME and the CNRS for funding and Dr. Markus Antonietti from the MPI of Colloids and Interface Sciences (Golm, Germany) for providing the KLE block copolymers. We also thank Dr. John Bass for his help with correcting the manuscript.

CM0706245